1D finite volume modelling of rarefaction wave propagation through a diaphragm using an added mass approach

C. Gianforcaro*,**, F. Bentivegna*, P. Galon*, F. Daude***,**** and C. Corre**
Corresponding author: camille.gianforcaro@cea.fr / camille.gianforcaro@ec-lyon.fr
* Université Paris-Saclay, CEA, Service d'Études Mécaniques et Thermiques, Gif sur Yvette, 91191, France
** Centrale Lyon, CNRS, Univ Claude Bernard Lyon 1, INSA Lyon, LMFA, UMR5509, Ecully, 69134, France
*** EDF Lab Paris-Saclay, ERMES - ElectRotechnique et MEcanique des Structures, Palaiseau, 91120, France
**** IMSIA, UMR EDF-CNRS-ENSTA 9219, Palaiseau, 91762, France

Abstract: Loss-of-primary-coolant accidents in pressurized water nuclear reactors involve the propagation of a rarefaction wave through an extended flow domain containing numerous geometric singularities (diaphragms, perforated plates, etc.). The efficient numerical simulation of such configurations relies on the simplified description of these singularities using an added mass source term in the governing equations. The present work focuses on the Finite Volume discretization of the modified hyperbolic system, namely the barotropic Euler equations with an added-mass term. Two approximate Riemann solvers (Rusanov and HLL) are developed for the modified system and assessed on a range of test cases, from a 1D shock tube to the reproduction of experiments carried out on the MADMAX platform. Comparisons with a 1D Finite Element discretization of the modified system, a 2D axisymmetric FV simulation with a discretization of the geometric singularities and experimental results allow to establish the Rusanov scheme is unable to provide physically accurate results as soon as the added-mass term varies in space. Meanwhile, the Finite Volume HLL scheme yields consistent results and provides a conservative alternative to the existing Finite Element approach.

Keywords: 1D Finite volume, Added mass, Loss-of-Coolant Accident, Unsteady pressure loss.

1. Context and motivation

The propagation of pressure waves through confined environments scattered with obstacles occurs across various engineering fields. Examples include investigating the impact of ventilation arrangements during an accidental hydrogen fuel cell explosion inside a ship [1], or mitigating micro-pressure waves generated when a high-speed train enters a tunnel equipped with retaining block structures [2]. The present work focuses on a loss-of-coolant accident (LOCA) scenario, where a rarefaction wave propagates through the pressure vessel of a pressurized water reactor (PWR) [3] (see Fig.1a). While the studies in [1] and [2] can rely on fully discretized meshes that resolve all geometric details of the domain, the sheer complexity and spatial scale of a PWR's entire primary loop during a LOCA renders such a strategy computationally unfeasible. To overcome this limitation, the methodology developed in [3], [4], and [5] relies on a coupled 1D/3D representation. In this approach perforated plates near the reactor core or diaphragms inside piping systems, are modeled in 1D using carefully calibrated local impedance relations [6, 7]. This approach is based on the assumption that the head loss created by these obstacles can be represented by two terms: one representing the steady head loss of the singularity, as given in [8] and another one representing the unsteady head loss—that is the effect of the singularity on the fluid's acceleration—and described by an inertial term. The MADMAX experimental setup, shown in Figs.1b and 1c, provides the empirical measurements required for this calibration process, as well as reference data for code validation.

Within the computationally efficient yet accurate simplified 1D approach, the impedance relations are currently implemented in the Finite Element (FE) framework of the EuroPlexus software [9] as an added mass term. The objective of the present study is to develop an equivalent simplified 1D approach within the Finite Volume (FV) solver of EuroPlexus. The expected benefit is to combine the conservation property of the FV method, which is desirable for this type of wave propagation problem, with the efficiency of an added mass formulation. To this end, Section 2 reviews the formulation of the added mass approach in the FV context, while Section 3 presents numerical results for a series of test cases, including a direct comparison with experimental data.

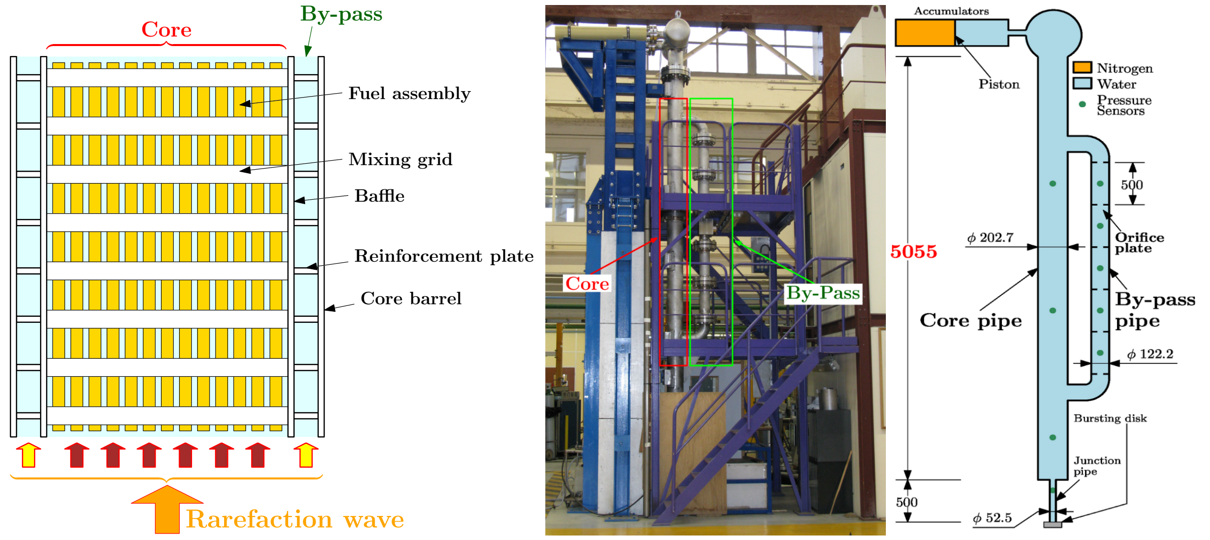

(a) (b) (c)

Figure 1: (a) Schematic view of the complex geometry through which the transient rarefaction wave propagates in a LOCA configuration [4]. (b) MADMAX experimental facility at DYN (CEA Saclay, France) designed to perform pressure measurements for a rarefaction wave propagating through a geometry representative of the core and by-pass regions found in the full LOCA configuration [4]. (c) Schematic diagram of the MADMAX facility [4].

2. Methodology

The added mass term used to model localized geometric details is introduced for the case of the 1D compressible Euler equations closed with a barotropic Equation of State (EoS). Then, a Finite Volume (FV) method is proposed for the resolution of the corresponding system. To this end, two approximate Riemann solvers, namely the Rusanov and the HLL schemes, are adapted to the modified Euler system including an added mass term.

2.1 Barotropic Euler equations

The 1D compressible barotropic Euler equations can be expressed as:

$$\begin{cases} \partial_t(\rho) + \partial_x(\rho u) & = 0 \\ \partial_t(\rho u) + \partial_x(\rho u^2 + p) & = 0 \end{cases} \tag{1}$$

where ρ is the fluid density, u the flow velocity, and p the pressure. Density and pressure are assumed to satisfy the following linear barotropic EoS:

$$p - p_0 = (\rho - \rho_0)\, c^2 \tag{2}$$

where ρ_0 and p_0 represent respectively the reference density and pressure while c is the speed of sound assumed to be constant here.

To account for localized geometric restrictions, an added mass term m_{add} is introduced into the Euler system so as to generate an inertial effect in the flow. We define $\overline{\rho}$ as the added density, constant in time and computed as m_{add} divided by the volume where the added mass is applied. This added density $\overline{\rho}$ is then introduced into (1) as an inertial source term in the momentum conservation equation:

$$\begin{cases} \partial_t(\overline{\rho}) & = 0 \\ \partial_t(\rho) + \partial_x(\rho u) & = 0 \\ \partial_t(\rho u) + \partial_x(\rho u^2 + p) & = -\partial_t(\overline{\rho} u) \end{cases} \tag{3}$$

Rewriting system (3) in conservative form yields:

$$\partial_t \mathbf{U} + \partial_x \mathbf{F} = 0 \quad \text{with } \mathbf{U} = \begin{bmatrix} \overline{\rho} \\ \rho \\ (\overline{\rho} + \rho) u \end{bmatrix} \text{ and } \mathbf{F} = \begin{bmatrix} 0 \\ \rho u \\ \rho u^2 + p \end{bmatrix} \tag{4}$$

The eigenvalues λ of the Jacobian matrix of the physical flux $\mathbf{F}$ are then computed:

$$\Rightarrow \begin{cases} \lambda^- = \dfrac{1}{2}\left[u\left(1 + \dfrac{\rho}{\overline{\rho}+\rho}\right) - \sqrt{u^2\left(1 - \dfrac{\rho}{\overline{\rho}+\rho}\right)^2 + \dfrac{4\rho c^2}{\overline{\rho}+\rho}} \right] \\ \lambda^0 = 0 \\ \lambda^+ = \dfrac{1}{2}\left[u\left(1 + \dfrac{\rho}{\overline{\rho}+\rho}\right) + \sqrt{u^2\left(1 - \dfrac{\rho}{\overline{\rho}+\rho}\right)^2 + \dfrac{4\rho c^2}{\overline{\rho}+\rho}} \right] \end{cases} \tag{5}$$

It can be observed that these eigenvalues are real and distinct for any physically admissible state, which implies that the modified system (3) remains strictly hyperbolic, mirroring the behavior of the classical system (1). Furthermore, in the limit where $\overline{\rho} = 0$, the eigenvalues correctly reduce to the classical acoustic wave speeds $\lambda^{\pm} = u \pm c$. Conversely, as $\overline{\rho} \to \infty$, the eigenvalues tend to $\lambda^{\pm} = \frac{1}{2}(u \pm |u|)$. Finally, it is straightforward to establish that the modified wave speeds are bounded by the standard acoustic speeds and satisfy $u - c \leq \lambda^- < \lambda^0 < \lambda^+ < u + c$. Furthermore, the eigenvectors of the system are expressed as follows:

$$\mathbf{w}^- = \begin{pmatrix} 0 \\ 1 \\ \frac{\lambda^- - u}{\rho c^2} \end{pmatrix} \quad , \quad \mathbf{w}^{\mathbf{0}} = \begin{pmatrix} 1 \\ 0 \\ 0 \end{pmatrix} \quad , \quad \mathbf{w}^+ = \begin{pmatrix} 0 \\ 1 \\ \frac{\lambda^+ - u}{\rho c^2} \end{pmatrix} \tag{6}$$

It can be shown that the waves associated with $\lambda^{\pm}$ and $\mathbf{w}^{\pm}$ are genuinely nonlinear, whereas the one associated with λ^0 and $\mathbf{w}^0$ is linearly degenerate. The final step in this mathematical development involves calculating the Riemann invariants $\mathcal{I}$ for this problem. They are determined using the following relation:

$$\nabla_{\mathbf{V}}(\mathcal{I}).\mathbf{w} = 0 \quad \text{with} \quad \nabla_{\mathbf{V}} = \left[\partial_{\overline{\rho}}, \partial_p, \partial_u\right] \tag{7}$$

For $\mathbf{w}^0$, we find that u and p (thus ρ as well because of the barotropic equation of state) are Riemann invariants, therefore these quantities do not vary during the passage of the wave associated with $\mathbf{w}^0$. For $\mathbf{w}^{\pm}$, $\overline{\rho}$ is invariant, implying that the added mass remains unchanged by the passage of waves associated with $\mathbf{w}^{\pm}$.

2.2 Numerical flux computations

The conservative formulation of the Finite Volume method requires the evaluation of a numerical flux at the interface between two adjacent control volumes. This numerical flux is typically computed by means of an approximate Riemann solver, which handles the local Riemann problem arising at the cell interfaces. The modifications introduced by the added mass term into the governing equations directly alter the wave propagation speeds, thereby affecting the structure of these Riemann solvers. Consequently, this section details the corresponding adaptations required for the numerical flux functions. In this work, attention is focused on two widely used approximate Riemann solvers: the Rusanov scheme and the HLL scheme.

2.2.1 Rusanov scheme

Using the mathematical analysis presented above, a Rusanov scheme [10] is built to calculate the numerical flux at the interface between two adjacent control volumes, denoted respectively by the index "$_L$" and "$_R$". Considering the Riemann problem associated with system (4), the Rusanov numerical flux $\mathcal{F}$ is given by:

$$\mathcal{F} = \frac{1}{2}\left(\mathbf{F}_L + \mathbf{F}_R - r_{\max}\left(\mathbf{U}_R - \mathbf{U}_L\right)\right) \tag{8}$$

where $r_{\max} = \max\left(r_L, r_R\right)$ represents the maximum spectral radius computed from the left and right states. Incorporating the modified eigenvalues, the local spectral radius r_K (for $K \in \{L, R\}$) is given by:

$$r_K = \frac{1}{2}\left[|u_K|\left(1 + \frac{\rho_K}{\overline{\rho}_K + \rho_K}\right) + \sqrt{u_K^2\left(1 - \frac{\rho_K}{\overline{\rho}_K + \rho_K}\right)^2 + \frac{4\rho_K c^2}{\overline{\rho}_K + \rho_K}}\right] \tag{9}$$

2.2.2 HLL scheme for barotropic equation of state

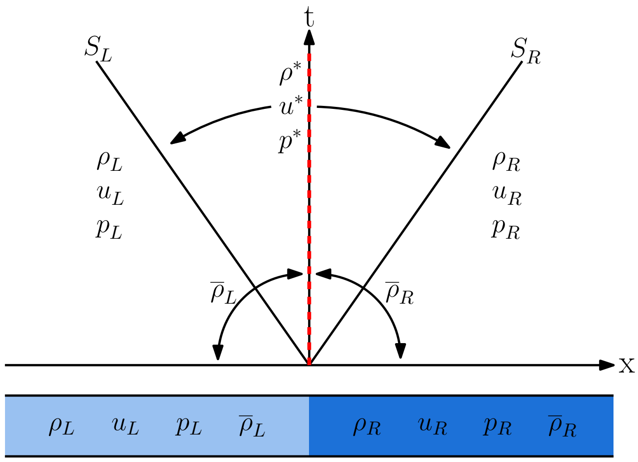

Figure 2: Representation of the Riemann problem in the x-t plane for the HLL solver. The discontinuities represented are either shock waves or rarefaction waves.

The HLL solver [11] provides a better approximation of the numerical flux compared to the Rusanov scheme. Here, its implementation for the modified barotropic system (4) is presented within the Riemann problem framework illustrated in Fig.2. We observe that since the added mass is constant in time, $\overline{\rho}$ remains unchanged across the S_L and S_R waves. A third vertical discontinuity appears, represented by the red dotted line, across which only $\overline{\rho}$ varies.

The HLL scheme assumes that the solution is constant between the left and right discontinuities of the problem, this region of the solution is denoted with the exponent "$*$". As previously shown, the left and right discontinuities are genuinely nonlinear within the framework of this system (4), so that one can apply the averaged Rankine-Hugoniot relation (with S_L and S_R respectively the propagation speeds of the left and right discontinuities):

$$\begin{cases} \mathbf{F}^* - \mathbf{F}_L = S_L\left(\mathbf{U}^* - \mathbf{U}_L\right) \\ \mathbf{F}^* - \mathbf{F}_R = S_R\left(\mathbf{U}^* - \mathbf{U}_R\right) \end{cases} \tag{10}$$

By combining these two relations, we can isolate an expression for the state $\mathbf{U}^*$ between the discontinuities:

$$\Leftrightarrow S_L\left(\mathbf{U}^* - \mathbf{U}_L\right) + \mathbf{F}_L = S_R\left(\mathbf{U}^* - \mathbf{U}_R\right) + \mathbf{F}_R \tag{11}$$

$$\Leftrightarrow \mathbf{U}^* = \frac{S_R\mathbf{U}_R - S_L\mathbf{U}_L + F_L - F_R}{S_R - S_L} \tag{12}$$

Substituting this expression back into (10) yields two expressions for $\mathbf{F}^*$, which allow us to obtain ρ^*, $(\rho u)^*$ and u^*. Finally, by once again making use of one of the relations in (10), we derive the numerical flux:

$$\mathcal{F} = \begin{pmatrix} F_1^* \\ F_2^* \end{pmatrix} = \begin{pmatrix} \frac{S_R\rho_L u_L - S_L\rho_R u_R + S_R S_L(\rho_R - \rho_L)}{S_R - S_L} \\ \frac{S_R p_L - S_L p_R + S_R\rho_L u_L^2 - S_L\rho_R u_R^2 + S_R S_L(\rho_R u_R - \rho_L u_L)}{S_R - S_L} + S_R S_L \frac{\overline{\rho}_R(u_R - u^*) - \overline{\rho}_L(u_L - u^*)}{S_R - S_L} \end{pmatrix} \tag{13}$$

It remains to estimate the values of S_L and S_R. A typical choice for HLL is to write:

$$S_L = \min\left(\lambda_L^-, \lambda_R^-\right) \tag{14}$$

$$S_R = \max\left(\lambda_L^+, \lambda_R^+\right) \tag{15}$$

Since λ depends on $\overline{\rho}$, a correct estimation of the wave velocities is achieved with the following expressions:

$$S_L = \min\left(\lambda_L^-(\overline{\rho}_L), \lambda_R^-(\overline{\rho}_L)\right) \tag{16}$$

$$S_R = \max\left(\lambda_L^+(\overline{\rho}_R), \lambda_R^+(\overline{\rho}_R)\right) \tag{17}$$

It is worth noting that when $\overline{\rho}_L = \overline{\rho}_R = 0$, the scheme degenerates into a classical HLL solution of the barotropic Euler equations. This behaviour is expected and confirms that the added mass has been properly taken into account in this approximate Riemann solver.

3. Numerical results

This section presents several test cases designed to validate the integration of the added mass term within the 1D Finite Volume framework. The numerical results are compared with validated 1D Finite Element solutions [5], 2D axisymmetric simulations, and available experimental data, ensuring a comprehensive assessment of the proposed methodology.

3.1 Shock tube

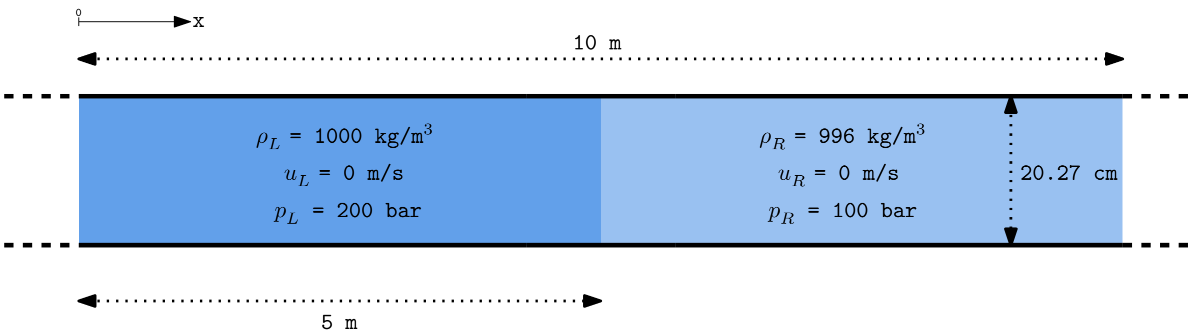

Figure 3: Schematic diagram of the 1D shock tube test case configuration.

The first numerical test case consists of a 10-meter-long shock tube, as schematically illustrated in Fig. 3. The left half is filled with a fluid of density $\rho_L = 1000\,\mathrm{kg.m^{-3}}$ and pressure $p_L = 200$ bar.

The right half, meanwhile, is filled with a fluid of density $\rho_R = 996$ kg.m^{-3} and pressure $p_R = 100$ bar. On both sides, the speed of sound is set to $c = 1500$ m/s. At the initial instant, the fluid is at rest, $u_L = u_R = 0$ m.s^{-1}.

To mimic an infinitely long pipe and prevent wave reflections, absorbing (non-reflecting) boundary conditions are prescribed at both ends of the computational domain. For this test case, the total added mass m_{add} is distributed uniformly across the entire domain volume, considering two values 0 kg and 1000 kg.

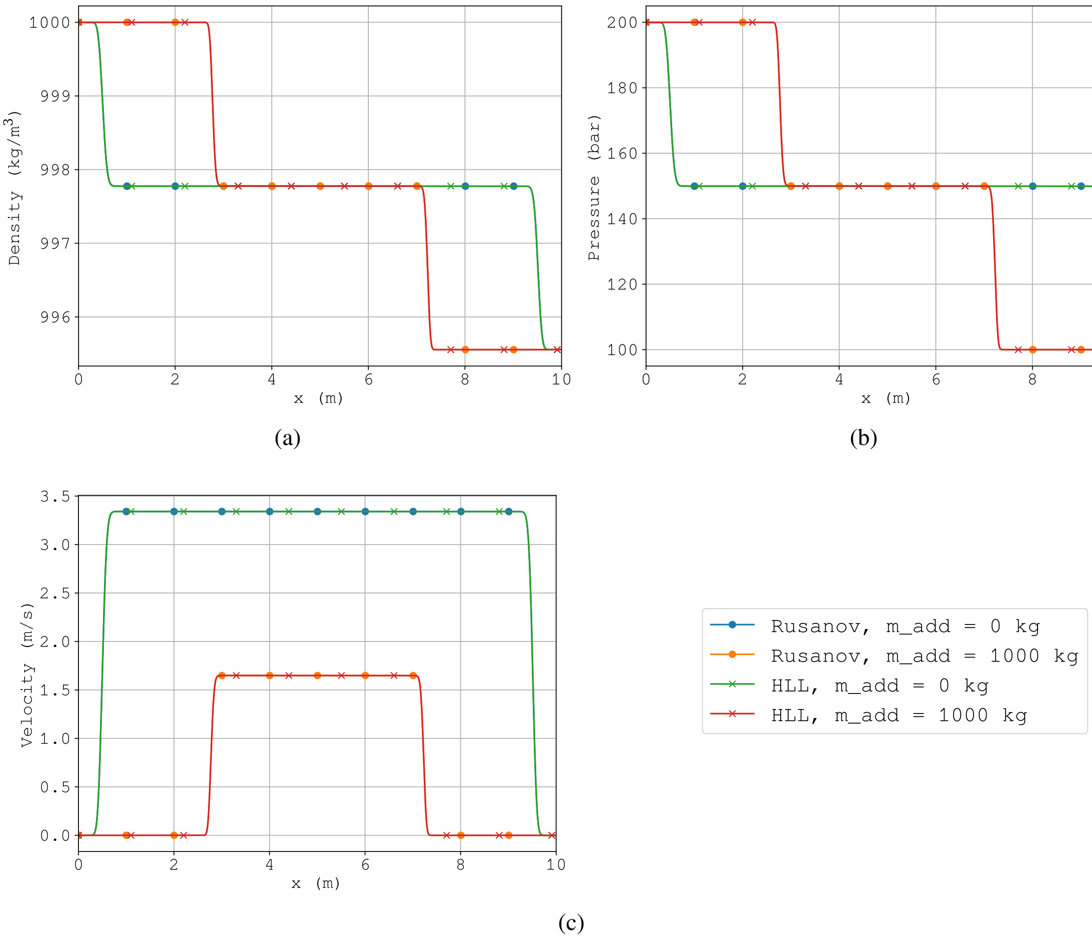

Figure 4: Numerical solutions for the 1D shock tube test case comparing added masses of 0 kg and 1000 kg using Rusanov and HLL Riemann solvers: (a) density, (b) pressure, and (c) velocity profiles. Simulations are performed with a CFL number of 0.9 and 1000 grid elements.

The numerical solutions displayed in Fig. 4 show the modified Rusanov and HLL formulations yield very consistent profiles, demonstrating the robustness of the added mass implementation across different Riemann solvers. Furthermore, the numerical results are in full agreement with the analysis conducted in Section 2. Specifically, the condition $u - c \leq \lambda^- < \lambda^+ \leq u + c$ is visually verified by the behavior of the transient fronts, as the introduction of the added mass significantly reduces the acoustic wave propagation speeds. Consequently, a marked reduction in the intermediate fluid velocity between the wave fronts is also observed, as illustrated in Fig. 4c.
To verify the accuracy of the numerical solutions, the results are compared against a simplified analytical validation based on a Joukowsky-type equation [12]:

$$\Delta p = \rho \alpha \Delta u \tag{18}$$

where Δp represents the pressure difference across the shock tube at the initial time, α is the wave propagation speed, and Δu is the velocity difference of the fluid on either side of one of the waves. Within the framework of the modified governing equations featuring an added mass term, the Joukowsky equation (18) can be extended as:

$$\Delta p = (\rho + \overline{\rho})\tilde{\alpha}\Delta\tilde{u} \tag{19}$$

Since adding mass to the system alters the wave propagation speed and the fluid velocity, the "~" notation is used in equation (19) to distinguish these values from those of the system without added mass in equation (18). Combining equations (18) and (19) gives:

$$\frac{\rho + \overline{\rho}}{\rho} = \mathcal{J} = \frac{\alpha\Delta u}{\tilde{\alpha}\Delta\tilde{u}} \tag{20}$$

where $\mathcal{J}$ is introduced as a characteristic dimensionless number. $\mathcal{J}$ can be estimated numerically using the right-hand side of (20). The left-hand side serves as an analytical solution. Varying the value of the added mass from 0 kg to 1000 kg, Fig.5 can be obtained.

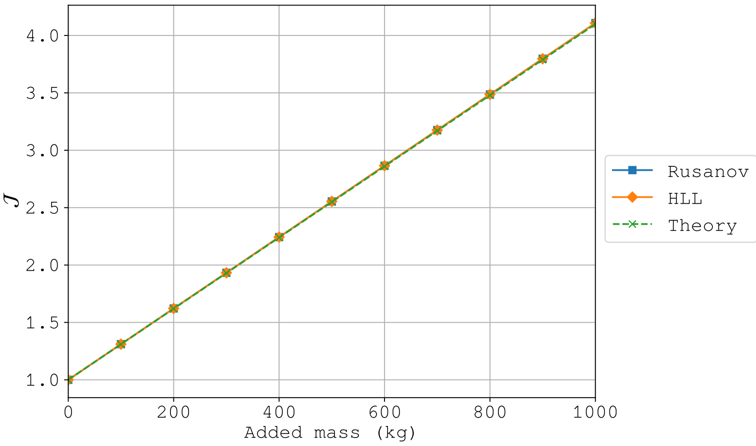

Figure 5: Comparison between the analytical and numerical values of $\mathcal{J}$ as a function of the added mass, ranging from 0 kg to 1000 kg.

As evidenced by the plots, the numerical results show excellent agreement with the analytical solution across the two implemented Riemann solvers. We therefore conclude that, for the shock tube test case, the numerical treatment of the added mass yields consistent results.

3.2 Shock tube with spatially varying added mass

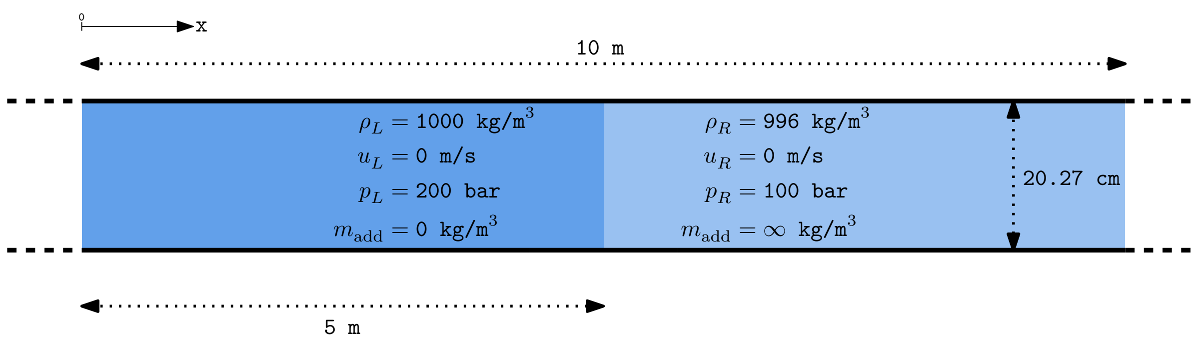

Figure 6: Schematic diagram of the 1D shock tube with spatially varying added mass test case.

The analytical expressions for the eigenvalues of the barotropic system (5) indicate that, in the case where the added mass is infinitely positive ($\overline{\rho} \to \infty$), we find $\lambda^{\pm} = \frac{1}{2}(u \pm |u|)$. Physically, a domain characterized by an infinite added mass is expected to behave as a wall on the flow.

To assess this behavior numerically, a benchmark test is designed using the same shock tube configuration as the previous case, but with the added mass strictly restricted to the right half of the tube ($x > 5$ m). To approximate the infinite mass limit, a large value of $m_{\text{add}} = 10^7$ kg is prescribed numerically.

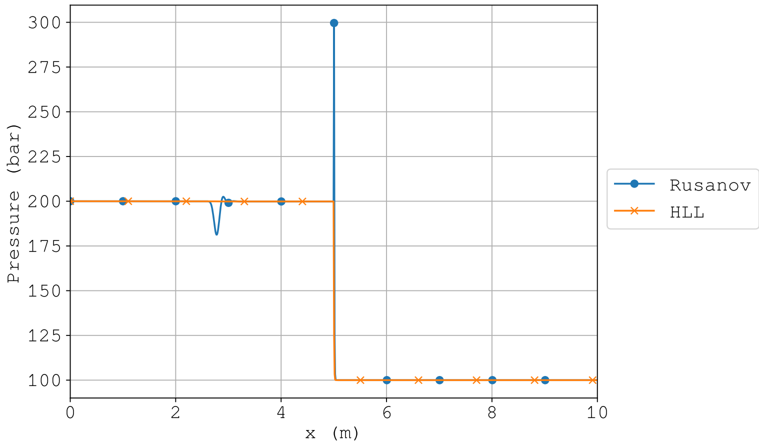

Figure 7: Pressure profiles of the shock tube with spatially varying added mass test case. The results were obtained using two different Riemann solvers: Rusanov and HLL. Simulations are performed with a CFL number of 0.9 and 1000 grid elements.

As shown in Fig.7 the HLL solver yields the expected solution: the right-hand side of the shock tube acts as a wall, preventing the fluid on the left-hand side—despite being subjected to a pressure twice greater—from propagating. At longer time steps, we nevertheless observe a diffusion of the discontinuity due to the fact that the added mass is not numerically infinite.
The Rusanov solver, on the other hand, does not yield the expected solution. Indeed, in addition to a pressure peak (300 bar) at the element forming the interface between the two domains of the shock tube, a wave is generated at the discontinuity and propagates into the left-hand side of the tube. The problem arises from the estimation of the spectral radius as Rusanov scheme assumes a certain symmetry in the problem, in the sense that r_L is of the same order of magnitude as r_R. However, at a jump in added mass, the difference between r_L and r_R is such that Rusanov scheme does not provide a satisfactory solution.

3.3 Passage of a rarefaction wave at an interface of added mass

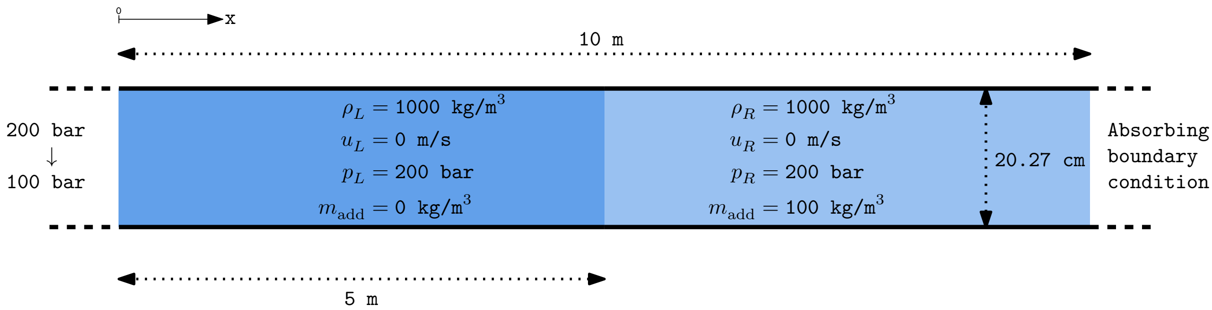

Figure 8: Schematic diagram of the passage of a rarefaction wave at an interface of added mass test case.

In this test case, we are approaching the targeted application scenario, as we are simulating the passage of a rarefaction wave through an added mass discontinuity. In the left half of the pipe, the added mass is null, while in the right half it is set to m_{add} = 100 kg. The density, velocity and pressure of the fluid are constant in the pipe at the initial time, see Fig.8. The rarefaction wave is generated by the left boundary condition, which imposes an instantaneous pressure drop from 200 to 100 bar.

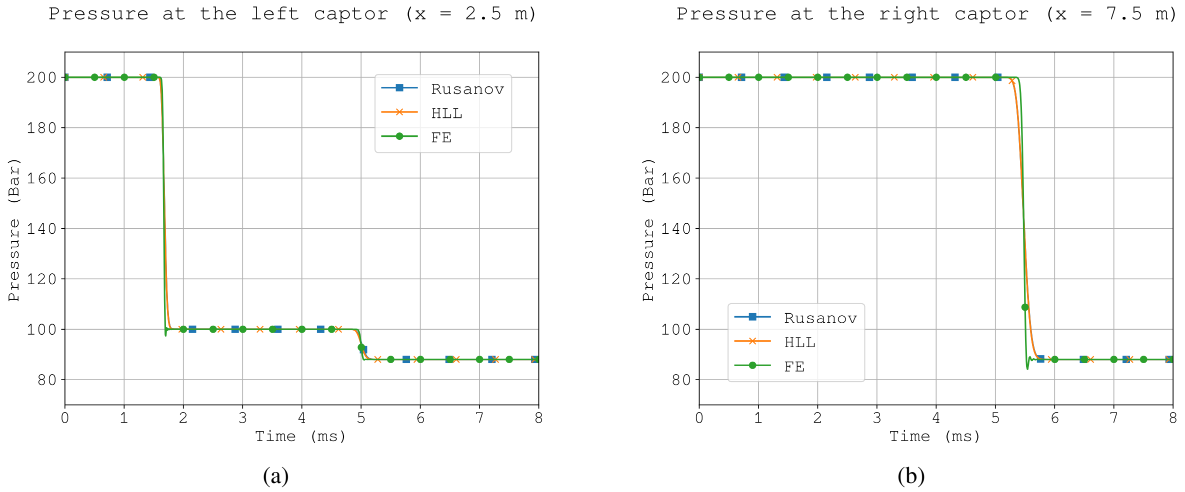

Figure 9: Pressure evolution for the passage of a rarefaction wave at an interface of added mass test case: (a) left sensor and (b) right sensor locations. The results were obtained using two different Riemann solvers (Rusanov and HLL) and a Finite Element solver. Simulations are performed with a CFL number of 0.9 and 1000 grid elements.

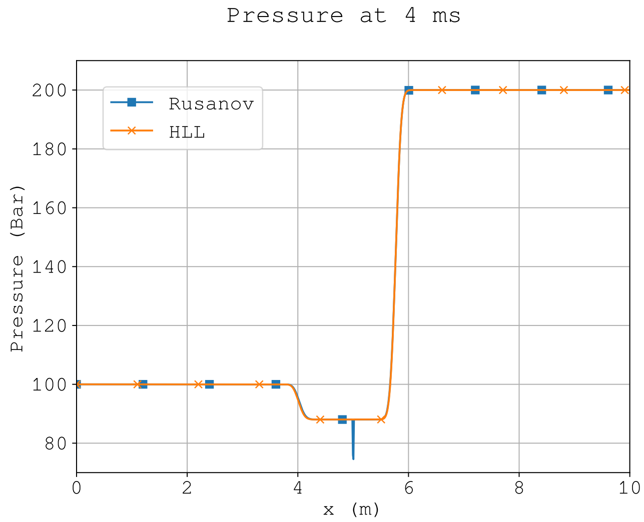

Figure 10: Pressure distribution for the passage of a rarefaction wave at an interface of added mass test case. The results were obtained using two different Riemann solvers: Rusanov and HLL. Simulations are performed with a CFL number of 0.9 and 1000 grid elements.

Fig.9 compares the results obtained using the finite volume method with the two developed Riemann solvers, Rusanov and HLL. The FV results are compared with those obtained using the finite element method, which, as mentioned above, has been validated by experimental comparisons. It can be seen in Fig.9a that all three simulations predict the same amplitude for the reflection of the incident wave. In Fig.9b, in addition to the previous observation, it can also be noted that the wave velocity in the medium with added mass is likewise the same, since the wave passes the sensor at the same time. Nevertheless, as shown in Fig.10, just as in the previous test case, the Rusanov scheme introduces a non-physical pressure peak at the added mass discontinuity.

3.4 Passage of a rarefaction wave in a diaphragm

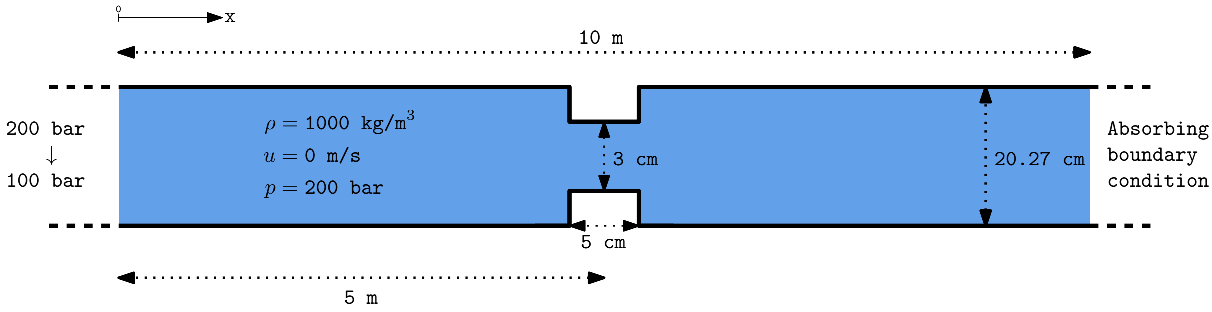

Figure 11: Schematic diagram of the passage of a rarefaction wave in a diaphragm test case.

Here we will discuss the simplified test case that most closely resembles the target application: the passage of a rarefaction wave through a diaphragm with an internal diameter of 3 cm and a thickness of 5 cm (Fig.11). As mentioned earlier, to represent this diaphragm in 1D, the model is decomposed into two parts. The unsteady part of the head loss is taken into account using an added mass which depends on the geometric characteristics of the diaphragm. The steady part, the so-called stationary head loss of the diaphragm, is calculated using a head loss coefficient k and is applied to the same element as the unsteady head loss, using a splitting method in the finite volume framework. To better appreciate the effects of the added mass in this test case, we will divide the analysis into two parts. First, a simulation in which only the added mass is taken into account will be discussed, followed by the complete model of the diaphragm.

3.4.1 Unsteady effect of the diaphragm

The value of the added mass required to model a diaphragm is given by [7] and [5] and reads:

$$m_{\text{add}} = (2+\alpha) S_p \rho_0 c \frac{\tau}{1 + {}^{\alpha}\!/_{2}} \tag{21}$$

with:

$$\alpha = \frac{1}{2} k \frac{u_0}{c} \qquad \tau = \frac{S_p}{S_d} \frac{L_{\text{eq}}}{2c} \qquad L_{\text{eq}} = 2 \left[0.85 - \frac{r_d}{r_p} + \left(0.15 \frac{r_d^2}{r_p^2} \right) \right] r_d + e \tag{22}$$

where S_p and S_p denote the cross-sectional areas of the pipe and the diaphragm respectively; similarly r_p and r_p denote the radius of the pipe and the diaphragm, e the thickness of the diaphragm, c the speed of sound in the fluid, ρ_0 the density of the fluid, k the head loss coefficient of the diaphragm and u_0 the fluid velocity at the initial instant. In this case, (21) gives $m_{\text{add}} = 104$ kg.
In this first part, we therefore simulate the propagation of a shock wave through a 10-meter-long pipe, in the middle of which an additional mass of 104 kg is placed on one element (at $x = 5$ m).

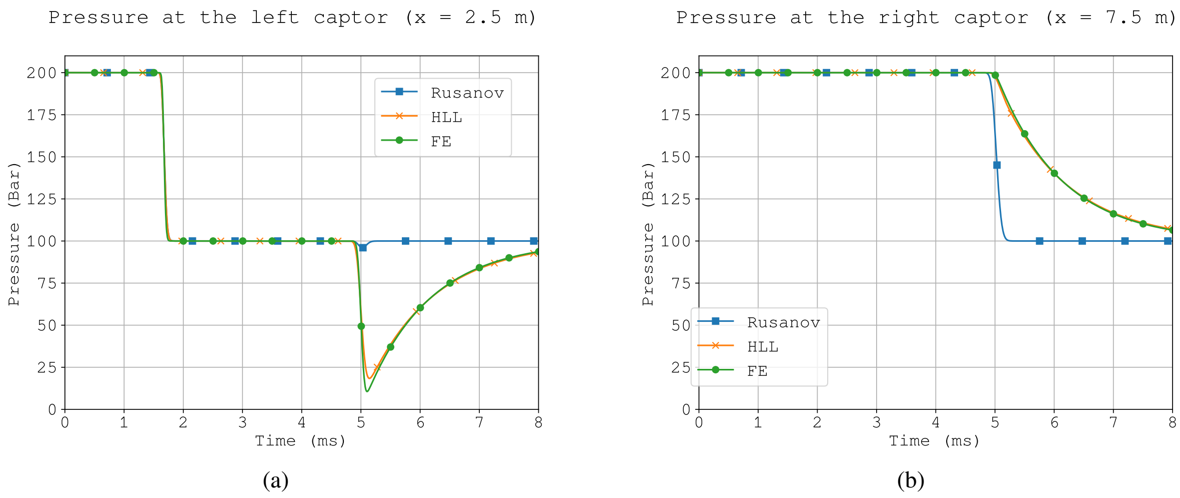

Figure 12: Pressure evolution of the passage of a rarefaction wave at an element with an added mass test case: (a) left (upstream) sensor and (b) right (downstream) sensor locations. The results were obtained using two different Riemann solvers (Rusanov, HLL) and a Finite Element solver. Simulations are performed with a CFL number of 0.9 and 1000 grid elements.

Fig.12 illustrates the effect of the added mass when used to model a diaphragm. Downstream of the added mass region (a single cell) (Fig.12b), it can be seen that the wave has been diffused. Upstream (Fig.12a), we observe that part of the wave is reflected by the diaphragm, after which the pressures on either side of the added mass equalize. The HLL finite volume result is close to the Finite Element results, slightly differing only in the prediction of the pressure minimum reached at 5 ms (see Fig.12a). This difference is due to the numerical diffusion in the finite volume scheme; a finer mesh allows to recover superimposed pressure evolutions for the Finite Element approach and the Finite Volume HLL scheme. Note that the Rusanov scheme does not allow to recover the targeted effects of the added mass. Upstream of the diaphragm, the reflection is minimal, while downstream the wave is barely diffused. As explained above, this is due to the Rusanov scheme's inability to process variations in added mass.

3.4.2 Steady and unsteady effect of the diaphragm

The steady head loss is calculated using the head loss coefficient k of the singularity, in this case the diaphragm. Here, we will use the formula given by [8]:

$$k = \left[\left(\frac{1}{2} + t\sqrt{1 - \frac{S_p}{S_d}}\right)\left(1 - \frac{S_p}{S_d}\right) + \left(1 - \frac{S_p}{S_d}\right)^2 + \Lambda\frac{e}{2r_d}\right]\left(\frac{S_p}{S_d}\right)^2 \tag{23}$$

with t a parameter dependent on the ratio of e over $2r_d$ (for this diaphragm, $t = 0.0617$) and Λ a parameter dependent on the Reynolds number of the flow, in this case, as viscosity is neglected, $\Lambda = 0$. We therefore find, for a diaphragm with an external diameter of 20.27 cm, an internal diameter of 3 cm and a thickness of 5 cm, a head loss coefficient $k = 3137$. By applying this steady head loss and the added mass of 104 kg, we obtain the results displayed in Fig.13, where the two Finite Volume schemes (Rusanov and HLL) are compared with a Finite Element result and a 2D axisymmetric Finite Volume computation.

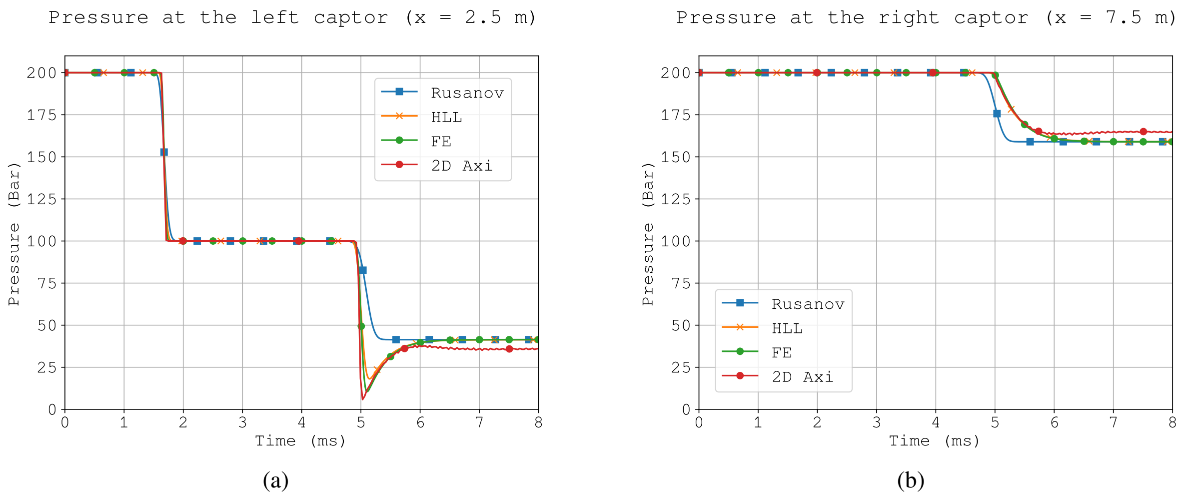

Figure 13: Pressure evolution of the passage of a rarefaction wave at an interface of added mass test case: (a) left sensor and (b) right sensor locations. 1D simulation are performed with a CFL number of 0.9 (expect for the Rusanov scheme which is at 0.7) and 1000 grid elements. Axisymmetric 2D simulation are performed with a CFL number of 0.4 and 244097 grid elements.

We first observe that all the methods, with the exception of the Rusanov scheme, provide the expected results. Upstream of the diaphragm (Fig.13a), we see the effect of the added mass discussed in section 3.4.1, but the pressure does no longer equalises with the downstream side of the diaphragm (Fig.13b). The steady head loss does indeed impose a pressure difference on both sides of the diaphragm. Furthermore the wave is also well diffused downstream of the added mass location.
For the Finite Volume Rusanov scheme, we observe once again that the effect of the added mass is not properly captured. The minimum pressure at 5 ms shown in Fig.13a is correctly predicted using the Finite Volume HLL scheme but a bit more diffuse with respect to the reference computations (2D axisymmetric and Finite Element with added mass). The 2D axisymmetric solution does not yield the same final pressure on either side of the diaphragm; it appears that this difference is linked to the 1D model and not specifically to the 1D finite volume method, since a similar problem is observed with the 1D finite elements.

3.5 MADMAX benchmark

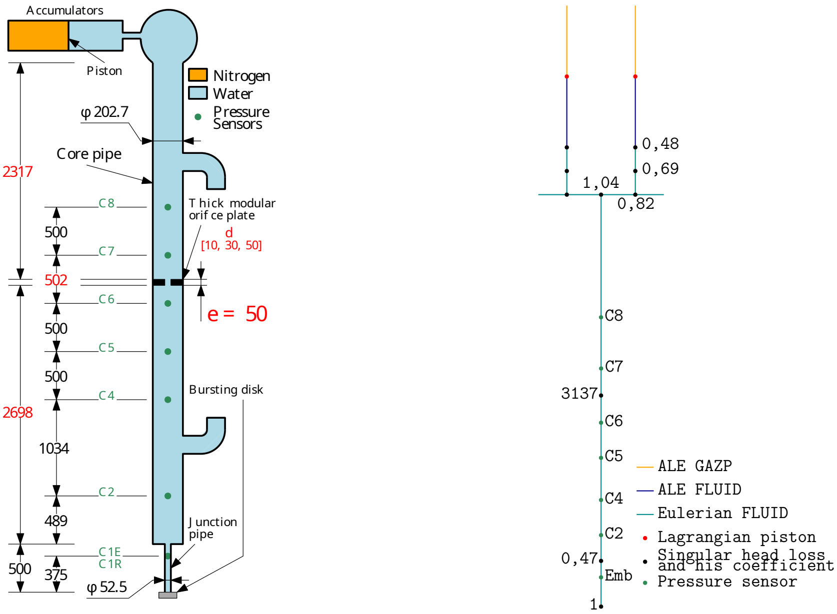

(a) (b)

Figure 14: (a) Schematic diagram of the simplified MADMAX configuration without by-pass pipe [5]. (b) Corresponding 1D simplified representation utilized in the numerical simulations.

As mentioned above, the MADMAX platform enables to experimentally validate the implementation of the diaphragm model. The configuration used here (see Fig.14a) consists of a main pipe with a diameter of 20.27 cm, in the middle of which is installed a diaphragm 5 cm thick and with an internal diameter of 3 cm. Two accumulators are placed at the top of the pipe, and at the bottom a graphite rupture disc ensures the creation of a rarefaction wave by breaking when the fluid pressure reaches approximately 70 bar. This experimental model is therefore represented in 1D by the diagram in Fig.14b, with each abrupt change in cross-section and bifurcation modelled by a head loss coefficient. The diaphragm, meanwhile, is modelled by an added mass (m_{add} = 104 kg) in addition to the head loss coefficient (k = 3137).

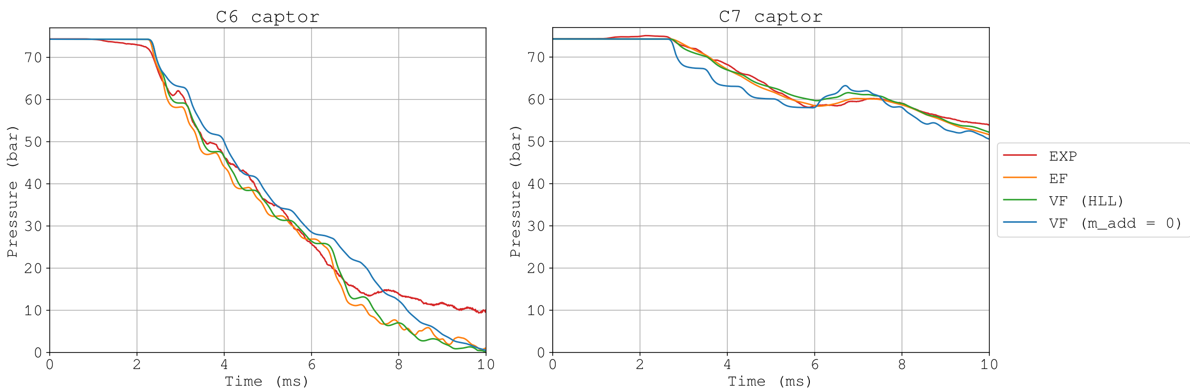

(a) (b)

Figure 15: Pressure evolution for the simplified MADMAX configuration evaluated at locations (a) upstream and (b) downstream of the diaphragm. The plots present a comparison between experimental measurements and the numerical results.

In order to assess more clearly the impact of the added mass, Fig.15 shows a HLL 1D finite volume simulation with and without the added mass, which is compared with the experimental values and a 1D finite element simulation. Upstream of the diaphragm (Fig.15a), the addition of mass allows the results to align much more closely with those of the finite element simulation and to approach the experimental values. The impact of the added mass becomes particularly apparent downstream of the diaphragm (see Fig.15b): it diffuses the wave passing through the diaphragm, thereby smoothing out the pressure changes. More generally, we observe that the Finite Volume model closely follows the experimental values and provides results similar to those given by the Finite Element approach, which was the main objective of this study.

4. Conclusion

In this paper, we have proposed a finite-volume methodology for solving the one-dimensional Euler barotropic equations including an added mass term to model localized geometric details in the flow domain. The modified hyperbolic system is solved using novel versions of the Rusanov and HLL numerical schemes, which reduce to their usual formulation for the baseline Euler system when the added mass term goes to zero. In the present work, the added mass is specifically used to model the effect of a geometric singularity, namely a diaphragm, on the flowfield properties during the propagation of a rarefaction wave. We have demonstrated, through numerical experiments, that the Rusanov scheme no longer provides an accurate solution when the distribution of the added mass varies in space. Using the proposed HLL scheme on a range of the increasingly complex test cases presented allowed us to confirm the validity of the FV methodology by successive comparisons with i) finite element results, for which the implementation of added mass is straightforward, ii) reference 2D axisymmetric simulations, and iii) experimental results provided by the MADMAX platform.
The assessment of the added mass formulation applied to the 1D Euler equations with total energy conservation is under way. It would be also valuable to expand in future work the library of approximate Riemann solvers extended to the modified 1D Euler equations with added mass. One open question remains regarding the possibility of extending the integration of added mass to cover multidimensional Euler equations as it could also be of interest.

References

[1] K. Ye, B. Zhang, Y. Xia, S. Zhang, B. Wang, Y. Ji, X. Wang, and W. Zhu. Numerical study on the influence of ventilation openings in marine hydrogen storage cabin on hydrogen deflagration. *Ocean Engineering*, 349:124189, 2026. doi:10.1016/j.oceaneng.2026.124189.

[2] F. Liu, M. Wei, H. Yang, W. Yang, and D. Chen. Numerical simulation and experimental study of the effects of retaining block structures on wavefront steepening in rail tunnels. *Journal of Wind Engineering and Industrial Aerodynamics*, 255:105956, 2024. doi:10.1016/j.jweia.2024.105956.

[3] V. Faucher, F. Crouzet, P. Piteau, P. Galon, and P. Izquierdo. Numerical and experimental analysis of transient wave propagation through perforated plates for application to the simulation of loca in pwr. *Nuclear Engineering and Design*, 253:1–11, 2012. SI : CFD4NRS-3. doi:10.1016/j.nucengdes.2012.08.009.

[4] F. Bentivegna, A. Beccantini, P. Galon, and C. Corre. Experimental and numerical analysis of rarefaction wave propagation across an orifice plate with varying thickness and diameter. *Mechanical Engineering Journal*, 11(2):23–00474–23–00474, 2024. doi:10.1299/mej.23-00474.

[5] F. Bentivegna. *Experimental and numerical analysis of fast transient flows in the presence of obstacles*. PhD thesis, Mécanique des fluides Ecully, Ecole centrale de Lyon 2024, 2024. Thèse de doctorat dirigée par Corre Christophe, Beccantini Alberto et Galon Pascal. URL: https://theses.fr/2024ECDL0026, doi:10.70675/0e74a850z21f7z450fz8f6fz50de4ece2f44.

[6] G. Baylac, R.J. Gibert, and M. Livolant. Calcul de l'amplification acoustique dans les circuits

complexes : application aux vibrations des échangeurs du réacteur chinon iii. *La Houille Blanche*, 57(5):407–428, 1971. arXiv:https://doi.org/10.1051/lhb/1971028, doi:10.1051/lhb/1971028.

[7] R.J. Gibert and B. Schwab. Étude de l'élément absorbant de Plexus en vue de représenter des plaques perforées traversées par une onde plane. Technical report, CEA, 1983.

[8] I. E. Idel'Cik. Memento des pertes de charge. *Collection de la Direction des Etudes et Recherches d'Electricité de France*, 1969.

[9] EUROPLEXUS Website, 2026. URL: http://www-epx.cea.fr.

[10] V. V. Rusanov. Calculation of interaction of non-steady shock waves with obstacles. *J. Comput. Math. & Phys. USSR*, 1:267–279, 1961.

[11] A. Harten, P. D. Lax, and B. van Leer. On upstream differencing and Godunov-type schemes for hyperbolic conservation laws. *SIAM Review*, 25(1):35–61, 1983. arXiv:https://doi.org/10.1137/1025002, doi:10.1137/1025002.

[12] N. Joukowsky. Über den hydraulischen stoss in wasserleitungsröhren. ("on the hydraulic hammer in water supply pipes."). *Mémoires de l'Académie Impériale des Sciences de St.-Pétersbourg*, 8th series (in German):1–71, 1898.